


Article

Study on Efficient Dephosphorization in Converter Based on Thermodynamic Calculation

Zhong-Liang Wang ¹, Tian-Le Song ¹, Li-Hua Zhao ^{2,*} and Yan-Ping Bao ^{1,*}

¹ State Key Laboratory of Advanced Metallurgy, University of Science and Technology Beijing, Beijing 100083, China

² School of Metallurgical and Ecological Engineering, University of Science and Technology Beijing, Beijing 100083, China

* Correspondence: zhaolihua@metall.ustb.edu.cn (L.-H.Z.); baoyyp@ustb.edu.cn (Y.-P.B.)

Abstract: Given the accelerating depletion of iron ore resources, there is growing concern within the steel industry regarding the availability of high-phosphorus iron ore. However, it is important to note that the utilization of high-phosphorus iron ore may result in elevated phosphorus content and notable fluctuations in molten iron, thereby imposing additional challenges on the dephosphorization process in steelmaking. The most urgent issue in the process of converter steelmaking is how to achieve efficient dephosphorization. In this study, the influence of various factors on the logarithm of the phosphorus balance distribution ratio ($\lg L_P$), the logarithm of the P_2O_5 activity coefficient ($\lg \gamma_{P_2O_5}$), and the logarithm of the phosphorus capacity ($\lg C_P$) were examined through thermodynamic calculations. The impact of each factor on dephosphorization was analyzed, and the optimal conditions for the dephosphorization stage of the converter were determined. Furthermore, the influence of basicity and FeO content on the form of phosphorus in the slag was analyzed using FactSage 7.2 software, and the precipitation rules of the slag phases were explored. The thermodynamic calculation results indicated that increasing the basicity of the dephosphorization slag was beneficial for dephosphorization, but it should be maintained below 3. The best dephosphorization effect was achieved when the FeO content was around 20%. The reaction temperature during the dephosphorization stage should be kept low, as the dephosphorization efficiency decreased sharply with the increasing temperature. In dephosphorization slag, $Ca_3(PO_4)_2$ usually formed a solid solution with Ca_2SiO_4 , so the form of phosphorus in the slag was mainly determined by the precipitation form and content of Ca_2SiO_4 . The phases in the dephosphorization slag mainly consisted of a phosphorus-rich phase, an iron-rich phase, and a matrix phase. The results of scanning electron microscopy and X-ray diffraction analyses were consistent with the thermodynamic calculation results.

Keywords: steelmaking; dephosphorization; thermodynamics; precipitation



Citation: Wang, Z.-L.; Song, T.-L.; Zhao, L.-H.; Bao, Y.-P. Study on Efficient Dephosphorization in Converter Based on Thermodynamic Calculation. *Crystals* **2023**, *13*, 1132. <https://doi.org/10.3390/cryst13071132>

Academic Editors: Daniel Medyński, Grzegorz Lesiuk and Anna Burduk

Received: 7 June 2023

Revised: 18 July 2023

Accepted: 19 July 2023

Published: 20 July 2023



Copyright: © 2023 by the authors. Licensee MDPI, Basel, Switzerland. This article is an open access article distributed under the terms and conditions of the Creative Commons Attribution (CC BY) license (<https://creativecommons.org/licenses/by/4.0/>).

1. Introduction

As the main raw material of the steel industry, iron ore is an important strategic resource for a country [1–4]. With the rapid development of iron and steel metallurgy technology, the demand for iron ore is increasing [5]. Iron ore resources are relatively abundant and widely distributed worldwide, but rich iron ore resources will gradually become depleted, so it is very important to develop and utilize iron ore with high phosphorus content [6]. During the sintering and blast furnace smelting process, the phosphorus in the ore will enter the sinter and hot metal [7–9]. Currently, steel companies have increasingly higher requirements for the quality of iron concentrates and strict limits on the phosphorus content, with the phosphorus content of iron concentrates required to be less than 0.024% [10]. There are many steel companies in China, and the differences in raw material conditions such as the phosphorus content of hot metal are significant among various steel mills. Only a few large steel companies in China can use high-quality iron ore with low

phosphorus content [11]. Many steel mills produce hot metal with a phosphorus content between 0.1 and 0.25%, and the phosphorus content in hot metal will further increase in the future [12].

The phosphorus in steel mainly comes from raw steelmaking materials such as hot metal, steel scrap, slagging materials, and deoxidizing alloys [13–15]. Phosphorus dissolves in the ferrite contained in steel [16]. It has a strong solid solution strengthening effect, significantly improving the strength and hardness of steel at room temperature. The strengthening effect of phosphorus is second only to carbon, which can significantly increase the yield strength and yield-to-tensile ratio of steel, but it also causes a significant decrease in plasticity and toughness (especially low-temperature toughness) and a sharp increase in the transition temperature of steel [17–19]. For most steel grades, phosphorus is a harmful element, so it is required to minimize the phosphorus content in the steel [20]. Dephosphorization is one of the most important functions in the converter steelmaking process, and the steel slag is the only place where phosphorus is removed from the steel. Converter dephosphorization mainly uses oxidation, which oxidizes the phosphorus in the steel to the slag phase under an oxidizing atmosphere to remove it [21]. The higher the phosphorus content in the hot metal, the greater the difficulty and technical requirements of the converter smelting process. Different conditions of phosphorus content in hot metal directly affect many key indicators such as the production rhythm of converter steelmaking, auxiliary material consumption, iron and steel material consumption, endpoint oxygen content, and endpoint accuracy rate [22–24]. As users' requirements for phosphorus content in steel become increasingly demanding, efficient dephosphorization in the converter has become the goal pursued by metallurgists. A large amount of research has been carried out at home and abroad on the dephosphorization reaction of steel, and a series of empirical and semi-empirical formulas have been obtained, which have certain guiding significance for actual production [25].

The removal trajectory of phosphorus involves the distribution between the steel and slag, as well as the distribution among different phases of slag. Therefore, to comprehensively understand the removal pattern of phosphorus in the converter and to obtain reasonable control conditions for the dephosphorization stage, it is necessary to consider both the reactions in the slag and the phase separation of dephosphorization slag. In this study, firstly, by using the thermodynamic empirical formulas summarized by previous researchers, the influence of different slag compositions and reaction temperatures on dephosphorization during slag–steel reactions was analyzed, and favorable control conditions for the dephosphorization stage of the converter were obtained. Then, based on the previous research, the form of phosphorus in the dephosphorization slag was analyzed, and the phase separation pattern of the dephosphorization slag was investigated. Industrial experiments were conducted to verify the thermodynamic calculation results, providing a research foundation for efficient dephosphorization in converters.

2. Research Method

The main factors affecting the dephosphorization effect of steel slag include the basicity of the slag; the contents of Fe_tO , MgO , MnO ; and the reaction temperature. Therefore, it is necessary to study the impact and degree of each factor on the dephosphorization ability of steel slag. The main parameters for evaluating the dephosphorization reaction were the phosphorus balance distribution ratio, the P_2O_5 activity coefficient, and the phosphorus capacity. Theoretical calculations were carried out based on thermodynamic formulas to analyze the influence of the main components and temperature of dephosphorization slag on the dephosphorization effect and to provide guidance for optimizing the converter dephosphorization process [26]. The contents of slag components in the dephosphorization stage of the converter used for calculation are shown in Table 1. By fixing the content of other components and adjusting the contents of CaO and SiO_2 in the slag while keeping the basicity of the slag unchanged, the impact of a single factor on the dephosphorization effect was studied. Additionally, since the dephosphorization reaction was an exothermic

process, the temperature was also an important factor affecting the dephosphorization efficiency. By examining the changes in the logarithm of the phosphorus balance distribution ratio ($\lg L_P$), the logarithm of the P_2O_5 activity coefficient ($\lg \gamma_{P_2O_5}$), and the logarithm of the phosphorus capacity ($\lg C_P$) under the influence of various factors, the impact of each factor on dephosphorization was determined, and the optimal conditions for the converter dephosphorization stage were analyzed. To avoid any misunderstandings, we wanted to clarify the nature of the logarithmic expressions used in thermodynamic calculations. These expressions did not originate from fundamental laws or principles but, rather, were the result of previous researchers' summarizations and inductions. The logarithmic functions served as mathematical tools in our thermodynamic calculations, allowing us to quantitatively evaluate the efficiency of phosphorus removal from slag. It is important to emphasize that these expressions should not be interpreted as representing inherent laws but rather to facilitate the analysis and interpretation of the computational results.

Table 1. Components of converter slag for calculation (%).

Composition	CaO	SiO ₂	Fe _t O	MnO	P ₂ O ₅	MgO
Content	38	19	25	5	3	10

2.1. Phosphorus Balance Distribution Ratio

The phosphorus distribution ratio between the slag and steel could well reflect the dephosphorization degree in the converter steelmaking process. The larger the phosphorus distribution ratio was, the better the dephosphorization effect was. As shown in Equation (1), this study cited the thermodynamic empirical formula for dephosphorization experiments in a CaO – Fe_tO – SiO₂ – MgO – MnO slag system summarized by Ide and Fruehan. to calculate the phosphorus distribution ratio [27]. In the equation, [%X] represents the content of X element in the steel liquid, in %, and (%X) represents the content of X element in the slag phase, in %. The expression for the phosphorus distribution ratio in the slag and steel was derived from Equation (1), as shown in Equation (2). By substituting the known composition of the furnace slag in Table 1 into Equation (2), the theoretical phosphorus balance distribution ratio under this condition can be calculated. The L_P was affected by factors other than the slag properties. Firstly, the activity coefficient of phosphorus in molten steel played a significant role in the distribution of phosphorus between the steel and slag. The activity coefficient was a parameter that described the activity of components in a molten system and was influenced by the concentration of phosphorus in the steel, the concentration of phosphorus in the slag, and the temperature. If the activity coefficient of phosphorus in the steel was relatively low compared to that in the slag, phosphorus tended to remain in the steel rather than combine with the slag. This led to a decrease in the L_P . Additionally, the oxygen potential (redox conditions) also affected the L_P . A higher oxygen potential promoted the formation of phosphorus oxide, while a lower oxygen potential facilitated the reduction of phosphorus, releasing it from the slag into the steel. Thus, variations in the oxygen potential altered the distribution of phosphorus between the steel and slag, thereby affecting the L_P . Other researchers have also summarized some empirical formulas for L_P , which were listed in Table 2. The main difference lay in the diverse calculation methods used for different slag systems. However, for the same slag system, it was recommended to choose an empirical formula that had been validated within the compositional range of the slag.

$$\lg \frac{(\%P)}{[\%P](\%T.Fe)^{2.5}} = 0.072[(\%CaO) + 0.15(\%MgO) + 0.6(\%P_2O_5) + 0.6(\%MnO)] + 11,570/T - 10.520 \quad (1)$$

$$\lg L_P = \lg \frac{(\%P)}{[\%P]} = 0.072[(\%CaO) + 0.15(\%MgO) + 0.6(\%P_2O_5) + 0.6(\%MnO)] + 11,570/T - 10.520 + 2.5 \lg(\%T.Fe) \quad (2)$$

Table 2. Common empirical formulas for L_P [27–33].

L_P Representation	L_P Calculation Formula
$\frac{(\%P_2O_5)}{[\%P]}$	$\lg L_P = 5.9(\%CaO) + 2.5\lg(\%FeO) + 0.5\lg(\%P_2O_5) - 0.5C - 0.36$ $\lg L_P = 0.072[(\%CaO) + 0.3(\%MgO) + 0.6(\%P_2O_5) + 0.2(\%MnO) + 1.2(\%CaF_2) - 0.5(\%Al_2O_3)]$ $+ 2.5\lg(\%T.Fe) + 11,570/T - 10.52$ $\lg L_P = \frac{1}{T} [162(\%CaO) + 127.5(\%MgO) + 28.5(\%MnO)] + \frac{11,000}{T} - 6.28 \times 10^{-4}(\%SiO_2) - 10.4$ $+ 2.5\lg(\%Fe_tO)$
$\frac{(\%P)}{[\%P]}$	$\lg L_P = \frac{22,350}{T} - 16 + 0.08(\%CaO) + 2.5\lg(\%T.Fe)$ $\lg L_P = 0.065[(\%CaO) + 0.55(\%MgO)] + 2.5\lg(\%T.Fe) + 12,230/T - 10.8$ $\lg L_P = 0.071[(\%CaO) + 0.1(\%MgO)] + 2.5\lg(\%T.Fe) + 8260/T - 8.56$ $\lg L_P = 0.073[(\%CaO) + 0.148(\%MgO) + 0.96(\%P_2O_5) + 0.144(\%SiO_2) + 0.22(\%Al_2O_3)] + 11,570/T$ $- 10.46 + 2.5\lg(\%T.Fe) \pm 0.1$

2.2. P_2O_5 Activity Coefficient

The activity coefficient of the slag component was one of the main factors affecting the thermodynamic properties of the slag. Phosphorus in the steel was oxidized and entered the steel slag in the converter, and the activity coefficient of P_2O_5 in the slag could significantly affect the dephosphorization effect of the steel slag. In this study, Equation (3) was cited, which assumed that phosphorus and oxygen in the steel liquid obeyed Henry's Law, and their activity coefficients were calculated as 1 [34]. Based on a large amount of experimental data, a linear relationship between the P_2O_5 activity coefficient ($\gamma_{P_2O_5}$) and the slag composition was regressed. Here, x_i represents the mole fraction of oxide i in the slag. By substituting the known slag composition in Table 1 into Equation (3), the P_2O_5 activity coefficient in the slag under the given conditions can be calculated.

$$\lg \gamma_{P_2O_5} = -22.44x_{CaO} - 15.3x_{MgO} - 13.26x_{MnO} - 12.24x_{Fe_tO} + 2.04x_{SiO_2} - 42,000/T + 23.58 \quad (3)$$

2.3. Phosphorus Capacity

Phosphate capacity (hereinafter referred to as P capacity) reflected the potential ability of steel slag to remove phosphorus. Since Wagner proposed the concept of P capacity and phosphide capacity, researchers had conducted extensive studies on the relationship between P capacity and slag composition. Many studies suggested that there was a good correlation between the P capacity of steel slag and its optical basicity, so P capacity could be used as a representation of slag basicity. This study cited the relationship between P capacity and optical basicity of various complex slags summarized by Bergman, as shown in Equation (4) [35]. The optical basicity Λ of the slag composed of various types of oxides was calculated using Equation (5), where m_i is the number of oxygen atoms in the oxide i and Λ_i is the theoretical optical basicity of the oxide, as shown in Table 3 [36]. The C_p referred to the ability of the slag to adsorb and combine with phosphorus at a given temperature. It was primarily determined by the properties of the slag, including its chemical composition, melting point, and structure. Therefore, at a fixed temperature, the C_p in steel was solely dependent on the properties of the slag and was not influenced by other factors.

$$\lg C_p = 21.55\Lambda + 32,912/T - 27.90 \quad (4)$$

$$\Lambda = \sum \frac{m_i x_i}{\sum m_i x_i} \Lambda_i \quad (5)$$

Table 3. Theoretical optical basicity of some oxides.

Oxide	CaO	SiO ₂	FeO	MnO	P ₂ O ₅	MgO
Optical basicity	1	0.47	0.72	0.95	0.38	0.92

2.4. Phase Precipitated Calculation

The high phosphorus distribution among the slag phases was a favorable driving condition for dephosphorization in the converter process. Through morphology and phase analysis of the slag, it was found that the slag mainly consisted of phosphorus-rich phase, iron-rich phase, and matrix phase. Phosphorus in the slag mainly existed in the phosphorus-rich phase and the matrix phase, and the enrichment of phosphorus in the phosphorus-rich phase had an important impact on the efficiency of dephosphorization in the converter process. Based on the composition of the slag during the converter process, this study used the Equilib module in the FactSage 7.2 thermodynamic software to calculate the phase precipitation process of the slag during the solidification process to investigate the influence of slag composition on phase precipitation in different slag systems. To ensure accurate calculations, we followed the recommended procedures provided by FactSage 7.2 for handling phosphorus-containing systems. This involved specifying the slag's elemental compositions, considering the interactions and phase stability of phosphorus-containing compounds, and utilizing the appropriate thermodynamic database within FactSage 7.2. This software has the advantages of having powerful calculation functions, rich database content, and a simple operating interface and has been widely used in thermodynamic simulation and calculation in the metallurgical field, achieving satisfactory results. The slag composition used for the theoretical calculation of phase precipitation is shown in Table 4.

Table 4. Components of converter slag for phase precipitation calculation.

No.	CaO	SiO ₂	Fe ₂ O ₃	MnO	P ₂ O ₅	MgO
1	28.5	28.5	25	5	3	10
2	38	19	25	5	3	10
3	42.75	14.25	25	5	3	10
4	48	24	10	5	3	10
5	44.67	22.33	15	5	3	10
6	41.33	20.67	20	5	3	10

3. Results and Discussion

3.1. Effect of Composition and Temperature on Dephosphorization

3.1.1. Basicity

The representation method for binary basicity in slag was $R = (\%CaO)/(\%SiO_2)$, and it had an important impact on the ability of slag to remove phosphorus. By fixing the content of other components in the slag, the basicity range of the slag was set to 1–4, and the impact of slag basicity on various dephosphorization indicators was analyzed. Figure 1 shows the effect of slag basicity on the three dephosphorization indicators lgL_p , $lg\gamma_{P_2O_5}$, and lgC_p . As the slag basicity increased, lgL_p and lgC_p increased, while $lg\gamma_{P_2O_5}$ decreased. CaO was a reactant in the dephosphorization reaction. Generally, when the slag basicity increased, the CaO content in the slag also increased. The increase in CaO content not only increased the concentration of the reactant in the dephosphorization reaction but also reduced $\gamma_{P_2O_5}$. Both effects increased the phosphorus distribution ratio, which was beneficial for dephosphorization. At the same time, as shown in Figure 1, as the basicity increased, the growth rate of lgL_p and lgC_p slowed down, and the decreasing trend of $lg\gamma_{P_2O_5}$ also slowed down. Therefore, although increasing the basicity of the converter slag was beneficial for dephosphorization, it inevitably increased lime consumption. If the basicity was too high, the effect of dephosphorization would not be significantly increased, and it could also lead to lime waste. Overall, when the slag basicity was less than 3, lgL_p and lgC_p increased rapidly, while $lg\gamma_{P_2O_5}$ decreased rapidly as the slag basicity increased. When the slag basicity exceeded 3, the growth rate of lgL_p and lgC_p slowed down, and the decreasing rate of $lg\gamma_{P_2O_5}$ also slowed down as the basicity increased. During the converter dephosphorization stage, if a large amount of lime was added to maintain a high slag basicity, a large amount of un-melted lime accumulated in the furnace, which not only worsened the dephosphorization kinetic conditions but also did not contribute

to dephosphorization due to the short time spent in the dephosphorization stage, and the smelting cost thus increased. Therefore, considering the comprehensive dephosphorization effect and steelmaking cost, the basicity of the converter slag during the dephosphorization stage should not exceed 3, and the effects of other factors on dephosphorization in this article were also calculated based on a basicity of no more than 3.

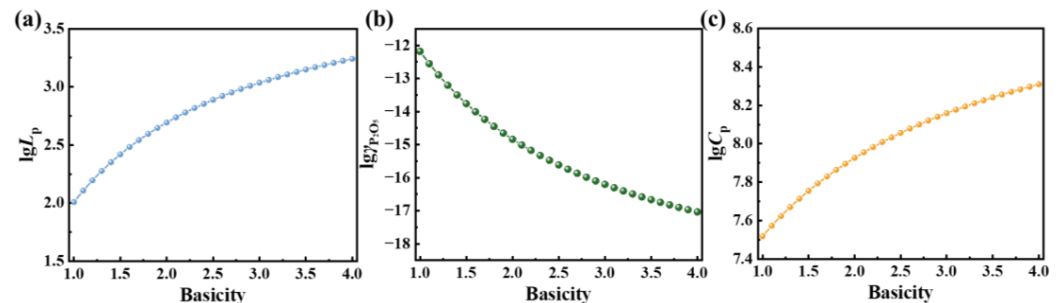


Figure 1. Effect of basicity on (a) $\lg L_p$, (b) $\lg \gamma_{P_2O_5}$, and (c) $\lg C_p$ in slag.

3.1.2. Fe_tO Content

The principle of dephosphorization in the converter was oxidation. The Fe_tO content in the slag had an important influence on dephosphorization and was a significant indicator of the oxidation capacity of the slag. The main method used to study the effect of Fe_tO content in the slag during the dephosphorization stage in the converter was to vary the Fe_tO content in the slag between 10 and 30% while keeping the other components in the slag constant. At the same time, the basicity of the slag was fixed at 1, 2, and 3, and the effect of Fe_tO content on dephosphorization in the slag at different basicity levels was analyzed. Figure 2 shows the effect of Fe_tO content in the slag on three dephosphorization indicators, $\lg L_p$, $\lg \gamma_{P_2O_5}$, and $\lg C_p$. It could be seen that as the Fe_tO content in the slag increased, $\lg \gamma_{P_2O_5}$ tended to increase linearly, and the higher the basicity, the more obvious the increase. $\lg C_p$ tended to decrease linearly, and the higher the basicity, the more obvious the decrease. Overall, when the Fe_tO content in the slag was around 20%, $\lg L_p$ was the largest, and both too high and too low Fe_tO contents are not conducive to dephosphorization. Fe_tO was a reactant in the dephosphorization reaction, and increasing its content could increase the oxygen potential in the slag, which was beneficial to dephosphorization. However, increasing the Fe_tO content in the slag would dilute the concentration of alkaline oxides in the slag, especially the concentration of CaO , and the higher the basicity, the more obvious the dilution effect, ultimately resulting in a decrease in $\lg C_p$ and an increase in $\lg \gamma_{P_2O_5}$.

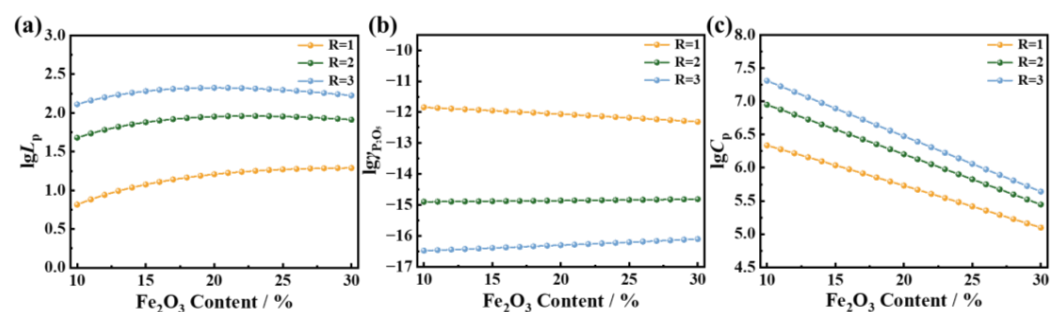


Figure 2. Effect of Fe_tO content on (a) $\lg L_p$, (b) $\lg \gamma_{P_2O_5}$, and (c) $\lg C_p$ in slag.

3.1.3. MgO Content

MgO was the main component for improving the refractoriness of slag. The main purpose of adding MgO to converter slag was to enhance the effect of slag splashing protection and maintain the condition of the converter. However, MgO in the slag also had certain ability to fix phosphorus. As MgO could combine with P_2O_5 to form phosphate, it had some impact on the dephosphorization ability of the slag. In order to analyze the

influence of the MgO content in the slag on the dephosphorization effect, the same method as above was adopted. The MgO content in the slag was varied between 1% and 11%, while the basicity and other component contents were kept constant. At the same time, in order to study the effect of MgO content on dephosphorization under different basicity levels, the basicity values were fixed at 1, 2, and 3. Figure 3 showed the influence of MgO content in the slag on three dephosphorization indicators, $\lg L_p$, $\lg \gamma_{P_2O_5}$, and $\lg C_p$. It could be seen that as the MgO content in the slag increased, $\lg L_p$ and $\lg \gamma_{P_2O_5}$ decreased linearly, while $\lg C_p$ increased linearly, and the change became more obvious with higher basicity. MgO itself was a weak alkaline substance, and its ability to fix phosphorus was not as good as CaO. CaO was the most important factor influencing $\lg L_p$, $\lg \gamma_{P_2O_5}$, and $\lg C_p$. The introduction of higher MgO content in the slag led to a consequent dilution of the concentration of CaO. As a result, the ability of CaO to effectively capture phosphorus decreased, leading to a reduction in $\lg L_p$ and $\lg \gamma_{P_2O_5}$. However, owing to its inherent basicity, the increase in MgO content caused $\lg C_p$ to increase. Adding a certain amount of MgO to the slag is necessary for dephosphorization and furnace lining protection, as it decreases the activity coefficient of P_2O_5 , thereby enhancing the dephosphorization process.

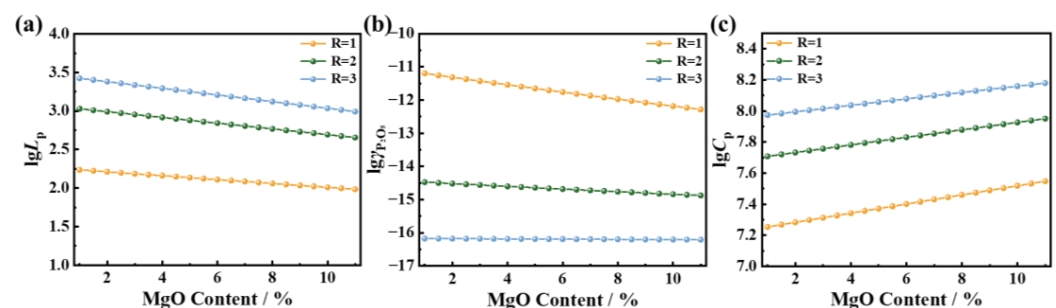


Figure 3. Effect of MgO content on (a) $\lg L_p$, (b) $\lg \gamma_{P_2O_5}$, and (c) $\lg C_p$ in slag.

3.1.4. MnO Content

The presence of MnO had a certain impact on the dephosphorization in the converter. In order to study its effect on dephosphorization, the same method as above was adopted to fix the content of other components in the slag and vary the MnO content in the slag within the range of 1–11%. At the same time, in order to study the effect of MnO content on dephosphorization under different levels of basicity, the basicity was fixed at 1, 2, and 3. Figure 4 showed the effect of MnO content in the slag on the three dephosphorization indicators $\lg L_p$, $\lg \gamma_{P_2O_5}$, and $\lg C_p$. It could be seen that as the MnO content in the slag increased, $\lg L_p$ and $\lg \gamma_{P_2O_5}$ decreased linearly, while $\lg C_p$ tended to increase linearly. The variation trend was similar to that of MgO. Because MnO was a weak alkaline substance, its ability to fix phosphorus was inferior to that of CaO. CaO was the most important influencing factor for $\lg L_p$, $\lg \gamma_{P_2O_5}$, and $\lg C_p$. The increase in the MnO content also diluted the concentration of CaO in the slag, resulting in a decrease in the phosphorus-fixing ability of CaO, leading to a decrease in $\lg L_p$ and $\lg \gamma_{P_2O_5}$ and an increase in $\lg C_p$. Therefore, the increase in the MnO content would reduce the dephosphorization ability of the slag, but its basicity would increase the phosphorus capacity of the slag. There would inevitably be a certain amount of elemental manganese in the molten iron, and the MnO content in the slag was mainly determined by the conditions of the molten iron.

3.1.5. Temperature

The dephosphorization reaction was a strongly exothermic reaction, so temperature had an important influence on dephosphorization. In order to study the effect of temperature on dephosphorization, the composition of the slag was kept constant, and the temperature was varied between 1200 °C and 1600 °C. In addition, in order to study the effect of temperature on dephosphorization under different levels of basicity, the basicity was fixed at 1, 2, and 3. Figure 5 shows the effect of temperature on the three dephosphorization

indicators $\lg L_p$, $\lg \gamma_{P_2O_5}$, and $\lg C_p$. As can be seen from Figure 5, as the temperature increased, $\lg L_p$ and $\lg C_p$ decreased significantly, while $\lg \gamma_{P_2O_5}$ increased sharply. Therefore, from a thermodynamic point of view, the reaction temperature during the dephosphorization stage of the converter should be reduced as much as possible. However, one of the main functions of the converter was to raise the temperature. If the temperature control during the dephosphorization stage was too low, the burden of raising the temperature during the decarbonization stage would be too heavy, which could not meet the requirements of steelmaking. Therefore, the temperature during the dephosphorization stage should be reduced as much as possible under the premise of meeting the requirements of steelmaking.

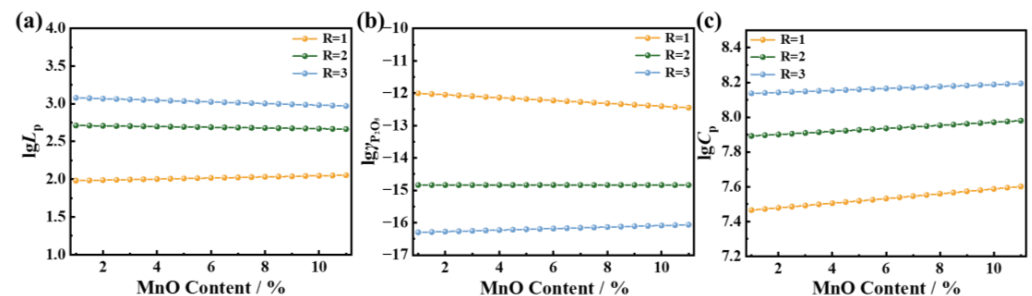


Figure 4. Effect of MnO content on (a) $\lg L_p$, (b) $\lg \gamma_{P_2O_5}$, and (c) $\lg C_p$ in slag.

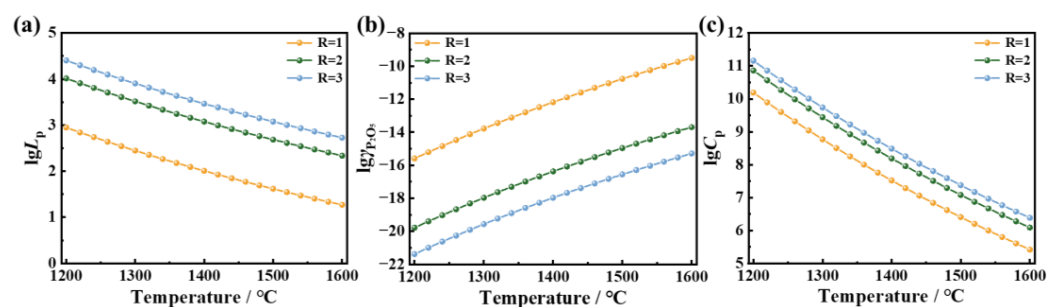


Figure 5. Effect of temperature on (a) $\lg L_p$, (b) $\lg \gamma_{P_2O_5}$, and (c) $\lg C_p$ in slag.

3.2. Effect of Steel Slag Composition on Precipitated Phase

3.2.1. Basicity

It was found from the above research that the most significant factors affecting the ability of dephosphorization from converter steel slag were basicity, Fe_tO content, and temperature. Therefore, FactSage 7.2 software was used to further analyze the effects of basicity and Fe_tO content on the phosphorus forms in the slag and explore the precipitation behavior of slag phases. Figure 6 shows the phase precipitation process of slag samples No. 1, No. 2, and No. 3 in Table 4 during the solidification process from 1700 °C to 700 °C. Figure 6a shows the phase precipitation of converter slag with a basicity of 1. The spinel phase began to precipitate at around 1350 °C and peaked at 1250 °C. At this time, the cordierite phase began to precipitate, which gradually decreased after peaking at 1180 °C. This was mainly due to Fe_tO entering the cordierite phase and forming $Ca_3Fe_2Si_3O_{12}$, the precipitation amount of which continued to increase with decreasing temperature until it reached the maximum value at 950 °C. The phosphorus-containing $Ca_3P_2O_8$ phase began to appear at 1090 °C, quickly reached the maximum value, and remained stable. Figure 6b shows the phase precipitation of converter slag with a basicity of 2. The $Ca_2Fe_2O_5$ phase began to precipitate at 1360 °C, and the $Ca_7MgSi_4O_{16}$ phase began to precipitate at 1270 °C, with its precipitation amount gradually increasing as the temperature decreased. When the temperature dropped to 1160 °C, the $Ca_7P_2Si_2O_{16}$ phase precipitated, and in the continued cooling process, this phase gradually decomposed to form a new phase, $Ca_5P_2SiO_{12}$, which remained stable. Figure 6c showed the phase precipitation of converter slag with basicity

of 3, which was basically the same as that of basicity 2. However, due to the lower SiO_2 content in the slag, the phosphorus-containing phase that finally formed was $\text{Ca}_4\text{P}_2\text{O}_9$.

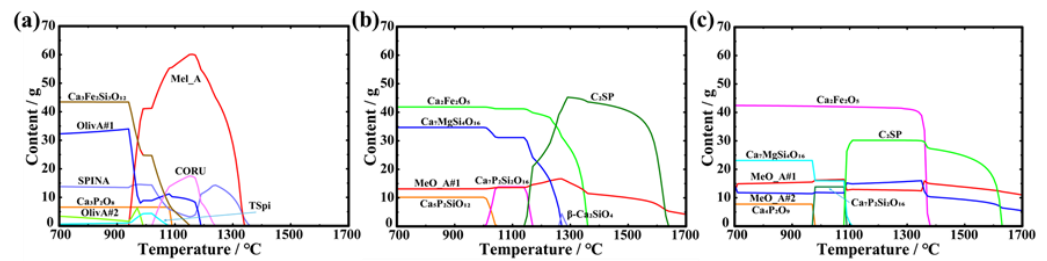


Figure 6. Calculation of phase precipitation in slag system: (a) No. 1, (b) No. 2, (c) No. 3.

3.2.2. Fe_tO Content

Figure 7 shows the phase precipitation process of slag samples No. 4, No. 5, and No. 6 in Table 4 during the solidification process from 1700 °C to 700 °C. Figure 7a presents the case of converter slag with 10% Fe_tO content. The $\alpha\text{-Ca}_2\text{SiO}_4$ phase began to precipitate at 1640 °C, and then underwent a crystal phase transition at 1400 °C, where $\alpha\text{-Ca}_2\text{SiO}_4$ disappeared and $\beta\text{-Ca}_2\text{SiO}_4$ began to precipitate. At the same time, the $\text{Ca}_7\text{MgSi}_4\text{O}_{16}$ phase started to precipitate in the slag at 1340 °C, and the precipitation amount continued to increase as the temperature decreased, reaching a maximum at 1100 °C. $\text{Ca}_2\text{Fe}_2\text{O}_5$ phase began to precipitate at 1260 °C. When the temperature dropped to 1190 °C, $\text{Ca}_7\text{P}_2\text{Si}_2\text{O}_{16}$ containing phosphorus began to precipitate. During the continued cooling process, this phase gradually decomposed and formed a new phase, $\text{Ca}_5\text{P}_2\text{SiO}_{12}$, which remained stable. Figure 7b presents the case of converter slag with 15% Fe_tO content. The $\alpha\text{-Ca}_2\text{SiO}_4$ phase began to precipitate at 1520 °C and then underwent a crystal phase transition at 1390 °C, where $\alpha\text{-Ca}_2\text{SiO}_4$ disappeared and $\beta\text{-Ca}_2\text{SiO}_4$ began to precipitate, but the precipitation amount was less than that of slag No. 4. Until 1350 °C, the precipitated $\beta\text{-Ca}_2\text{SiO}_4$ gradually reacted with the slag, causing the precipitation amount of $\text{Ca}_7\text{MgSi}_4\text{O}_{16}$ phase to gradually increase. The transformation of the phosphorus-containing phase was basically the same as that of slag No. 4, and eventually became the $\text{Ca}_5\text{P}_2\text{SiO}_{12}$ phase. Figure 7c presents the case of converter slag with 20% Fe_tO content. In this slag, the precipitation amount of $\alpha\text{-Ca}_2\text{SiO}_4$ was small, and no crystal phase transition occurred. The $\text{Ca}_3\text{MgSi}_2\text{O}_8$ phase began to precipitate at 1400 °C, and reached a maximum at 1350 °C, before quickly transforming into the $\text{Ca}_7\text{MgSi}_4\text{O}_{16}$ phase. The phosphorus-containing phase that finally stabilized in the slag was also $\text{Ca}_5\text{P}_2\text{SiO}_{12}$.

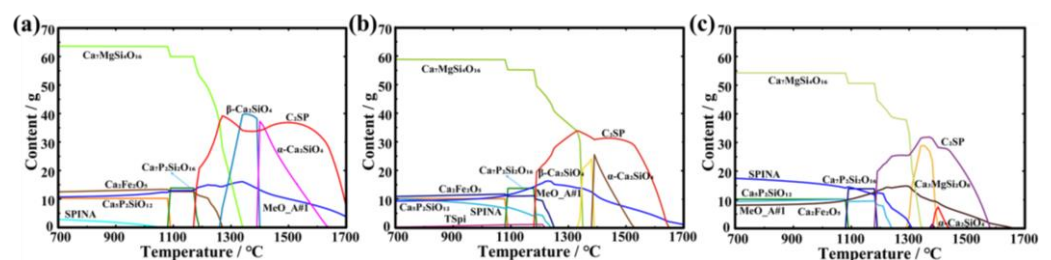


Figure 7. Calculation of phase precipitation in slag system: (a) No. 4, (b) No. 5, (c) No. 6.

3.3. Industrial Experiment Verification

In pursuit of faster production rhythms, the converter smelting process was usually operated continuously, as shown in Figure 8. Scrap steel was loaded as the starting point for smelting, followed by molten iron. Then, rapid blowing was carried out using a porous oxygen lance, and slag-making auxiliary materials were added. The oxygen supply time varied depending on the size of the converter but was generally around 20 min. The blowing lance was generally operated in a low–medium–high–low mode and adjusted according to the slag formation inside the furnace during production. Then, the steel was

tapped into a ladle for further treatment. After pouring the steel, nitrogen was used for slag splashing to protect the furnace, and finally, the slag was tapped out. The most pressing issue in actual production is how to remove phosphorus from the molten iron and fix it in the slag within a short amount of time. Based on the previous theoretical calculations, it is necessary to ensure a relatively high basicity of the slag during the phosphorus removal stage in the converter while maintaining sufficient fluidity. Additionally, the content of Fe_tO , MgO , and MnO in the steel slag also has a certain influence on phosphorus removal. Therefore, in the smelting process using the single-slag method, controlling the basicity of the converter slag at around 2.5 and the Fe_tO content at approximately 20% achieves the optimal phosphorus removal effect. The composition of the slag at this stage is shown in Table 5, and micro-area morphology observation and XRD phase analysis were performed. Each slag sample is quenched in water at approximately 1000 °C to ensure consistency in the cooling process. The results presented are the average values obtained from these three samples, aiming to enhance the reliability of the findings despite the constraints in obtaining a larger quantity of samples in an industrial setting.

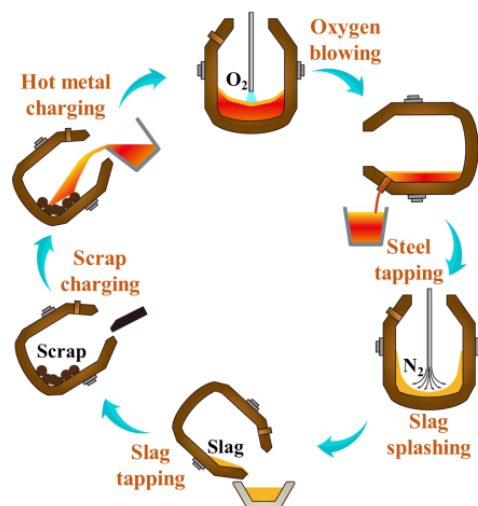


Figure 8. Production process of converter steelmaking process.

Table 5. Components of converter slag sampled on site.

Composition	CaO	SiO_2	Fe_tO	MnO	P_2O_5	MgO
Content	39.1	15.5	21.2	6.8	3.3	7.7

Figure 9a,b are backscattered electron micrographs of the dephosphorization slag which clearly showed the presence of three distinct phases: the phosphorus-rich phase, the iron-rich phase, and the matrix phase. Typically, the phosphorus-rich phase in the converter slag predominantly exists as the $\text{Ca}_5\text{P}_2\text{SiO}_{12}$ phase, and phosphorus mainly resides in this phase, which appears as a dark gray color in the micrograph. The iron-rich phase in the slag typically appears as white in scanning electron microscopy and is mainly composed of iron oxide or iron–manganese oxide. The matrix phase appears as gray and contains elements that had not fully entered either the phosphorus-rich or iron-rich phases. Figure 9c presents the XRD pattern of the experimental slag, which mainly consists of five phases: $\text{Ca}_5\text{P}_2\text{SiO}_{12}$, $\text{Ca}_2\text{Fe}_2\text{O}_5$, FeS , $(\text{MnO})_{0.165}(\text{CaO})_{0.835}$, and FeO . These phases are in good agreement with the calculated results of the precipitates in Figure 7c, with the final phosphorus-containing phase being $\text{Ca}_5\text{P}_2\text{SiO}_{12}$.

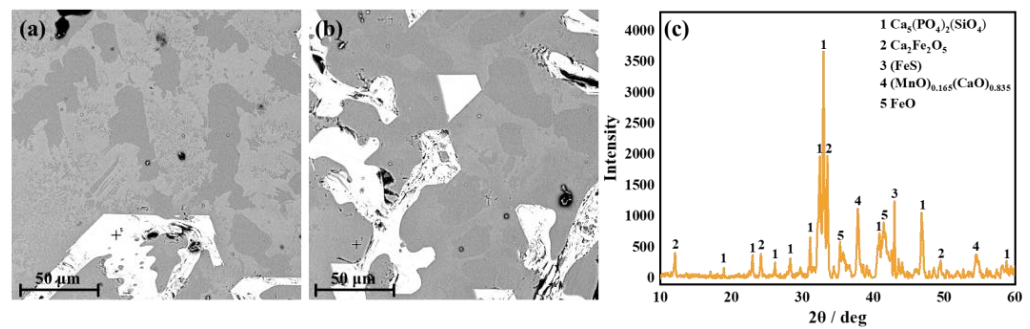


Figure 9. (a,b) Microscopic morphology and (c) XRD pattern of slag in converter dephosphorization stage.

In order to investigate the phosphorus distribution ratio in practical production scenarios, we conducted compositional measurements on 15 sets of steel slag samples and their corresponding steel liquid compositions in Table 6. These samples were directly obtained from the production site, ensuring their relevance to real-world conditions. By analyzing the collected data and building upon the existing Equation (2), we were able to summarize and derive a new Equation (6). The computations were performed using the SPSS 25.0 software (Statistical Package for the Social Sciences), a widely used tool for statistical analysis. The p -values for each coefficient were calculated using Spearman's correlation analysis and are presented in Table 7. All coefficients demonstrated statistical significance with p -values less than 0.05, passing the significance test. Additionally, the equation achieved a high R^2 value of 0.905, indicating a strong fit and excellent predictive performance. This revised equation provides an accurate prediction of the phosphorus distribution ratio between the slag and steel liquid during the dephosphorization process. Our equation is primarily developed for a specific research object, namely a 100-ton converter in a particular steel plant, and therefore, it does not possess universal applicability. It is important to note that different equipment conditions and operational processes have a significant impact on phosphorus partitioning ratios, as these parameters influence the extent of the phosphorus removal reactions. Furthermore, it should be emphasized that the derived equation does not represent the phosphorus partitioning at long-term equilibrium. In our specific study, the overall duration of the converter process is approximately 30 min, with a phosphorus removal reaction time of less than 10 min for the molten steel. Consequently, the equation we have derived reflects the non-equilibrium conditions prevailing during the relatively short time span of the converter process. The equation has been validated extensively within a suitable range of basicity, which spans from 1.3 to 2.4, and a temperature range of 1300 to 1450 °C. The accuracy of the equation has been thoroughly verified within these specified ranges. Therefore, we can ensure the reliability of the equation within these validated conditions. Figure 10 presents the comparison between the measured phosphorus partitioning ratios and the predictions obtained using different equations. It can be observed that the predictions obtained using Equation (6) exhibit a small deviation from the measured values, indicating a good agreement. However, the predictions obtained from the other three equations deviate significantly from the measured values. These discrepancies can be attributed to the non-equilibrium state during the phosphorus removal process in the converter and the incomplete phosphorus removal due to the insufficient effectiveness of lime in the slag.

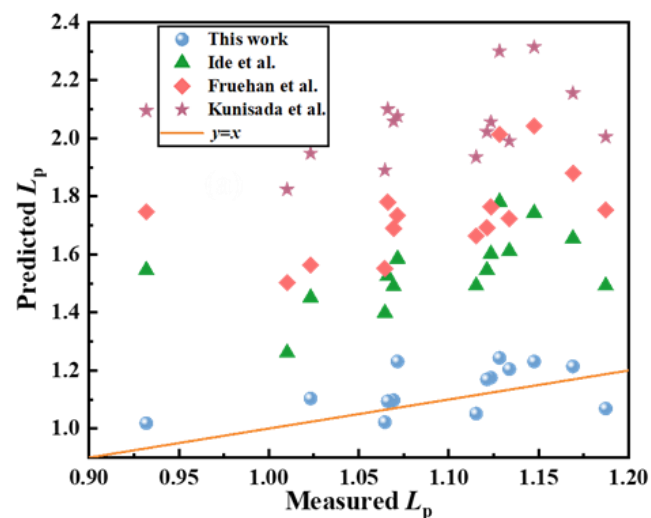
$$\lg L_P = \lg \frac{(\%P)}{[\%P]} = 0.072[0.8(\%CaO) + 0.35(\%MgO) + 0.7(\%P_2O_5) + 0.8(\%MnO)] + 11,570/T - 10.620 + 2.5\lg(\%T.Fe) \quad (6)$$

Table 6. Common empirical formulas for L_p .

No.	Main Components of Dephosphorization Slag/%						[P] Content in Molten Steel/%	Temperature/°C
	CaO	SiO ₂	Fe _t O	MnO	P ₂ O ₅	MgO		
1	32.6	18.1	25.3	5.4	3.7	7.7	0.137	1332
2	31.8	19.5	27.7	5.7	3.8	5	0.143	1400
3	37.2	21.2	18.9	6.1	4.3	5.3	0.144	1375
4	35.8	18.8	22.5	3.8	4.9	7.1	0.139	1386
5	34.8	20.7	24.4	6.1	4.2	3.9	0.138	1367
6	32.8	17	29.4	3.9	3.6	6.8	0.134	1393
7	36.8	17.2	23.7	4.2	4.8	6.5	0.142	1377
8	37.9	19.4	25.3	2.9	4.6	4.1	0.143	1368
9	34.2	19	26.9	3.4	4	5.8	0.15	1378
10	42	18.1	18.2	4.1	4.4	5.3	0.143	1354
11	33.6	15.8	26	5.3	4.3	6.9	0.142	1380
12	38.2	20.3	16	7.3	4.3	7.4	0.138	1327
13	42.3	22.3	14.6	4.9	2.8	6.3	0.143	1352
14	32.2	23.6	23.3	4.4	3.4	4.6	0.145	1368
15	31.3	15.7	28.5	5.6	3.6	6.7	0.149	1383

Table 7. Spearman correlation analysis results for coefficients.

Coefficient	(%CaO)	(%MgO)	(%P ₂ O ₅)	(%MnO)	1/T	lg(%T.Fe)
<i>p</i> -value	0.000	0.011	0.000	0.003	0.006	0.000

**Figure 10.** Measured and predicted phosphorus partitioning ratios using different equations [27,32,33].

4. Conclusions

This study investigated the behavior of steel slag during the dephosphorization stage in the converter process using thermodynamic calculations and sampling analysis. The optimal thermodynamic conditions for this stage were obtained and provide a certain reference for practical production. The following conclusions were drawn:

1. The results of thermodynamic formula calculations showed that increasing the basicity of the dephosphorization slag was beneficial for dephosphorization, but it should be kept below 3. When the Fe_tO content was around 20%, the dephosphorization effect was the best, and a too high or too low Fe_tO content was not conducive to dephosphorization. The contents of MgO, MnO, and other components had little effect on the dephosphorization effect. The reaction temperature should be kept relatively low during the dephosphorization stage, and the dephosphorization efficiency sharply decreased with the increase in temperature.

2. During the solidification process of the dephosphorization slag, phosphorus existed in the form of $\text{Ca}_3(\text{PO}_4)_2$. When the slag basicity and Fe_tO content changed, $\text{Ca}_3(\text{PO}_4)_2$ only changed its precipitation form, but the precipitation amount remained unchanged. $\text{Ca}_3(\text{PO}_4)_2$ in the slag usually formed a solid solution with Ca_2SiO_4 , so the form of phosphorus in the slag was mainly determined by the precipitation form and content of Ca_2SiO_4 .
3. The phases in the dephosphorization slag were mainly composed of phosphorus-rich phases, iron-rich phases, and the matrix phase. This was consistent with the results of scanning electron microscopy observation and XRD analysis. The developed prediction model accurately estimates the phosphorus distribution ratio between the slag and steel liquid.

Author Contributions: Conceptualization, Z.-L.W. and T.-L.S.; methodology, L.-H.Z.; software, T.-L.S.; validation, Z.-L.W., Y.-P.B. and L.-H.Z.; funding acquisition, Y.-P.B. All authors have read and agreed to the published version of the manuscript.

Funding: This research was funded by the National Natural Science Foundation of China, grant number 51574019.

Data Availability Statement: Not applicable.

Conflicts of Interest: The authors declare no conflict of interest.

References

1. Hao, X.; An, H. Comparative study on transmission mechanism of supply shortage risk in the international trade of iron ore, pig iron and crude steel. *Resour. Policy* **2022**, *79*, 103022. [\[CrossRef\]](#)
2. Ma, S.; Wen, Z.; Chen, J.; Wen, Z. Mode of circular economy in China's iron and steel industry: A case study in Wu'an city. *J. Clean. Prod.* **2014**, *64*, 505–512. [\[CrossRef\]](#)
3. Zhang, Q.; Sun, Y.; Han, Y.; Li, Y.; Gao, P. Review on coal-based reduction and magnetic separation for refractory iron-bearing resources. *Int. J. Miner. Metall. Mater.* **2022**, *29*, 2087–2105. [\[CrossRef\]](#)
4. Wang, Z.; Bao, Y.; Wang, D.; Wang, M. Effective removal of phosphorus from high phosphorus steel slag using carbonized rice husk. *J. Environ. Sci.* **2023**, *124*, 156–164. [\[CrossRef\]](#) [\[PubMed\]](#)
5. Lawrence, K.; Nehring, M. Market structure differences impacting Australian iron ore and metallurgical coal industries. *Minerals* **2015**, *5*, 473–487. [\[CrossRef\]](#)
6. Sun, Y.; Han, Y.; Gao, P.; Wang, Z.; Ren, D. Recovery of iron from high phosphorus oolitic iron ore using coal-based reduction followed by magnetic separation. *Int. J. Miner. Metall. Mater.* **2013**, *20*, 411–419. [\[CrossRef\]](#)
7. Liu, X.; Feng, H.; Chen, L.; Qin, X.; Sun, F. Hot metal yield optimization of a blast furnace based on constructal theory. *Energy* **2016**, *104*, 33–41. [\[CrossRef\]](#)
8. Zhu, D.; Yang, C.; Pan, J.; Lu, L.; Guo, Z.; Liu, X. An integrated approach for production of stainless steel master alloy from a low grade chromite concentrate. *Powder Technol.* **2018**, *335*, 103–113. [\[CrossRef\]](#)
9. Chen, Y.; Zuo, H. Gasification behavior of phosphorus during pre-reduction sintering of medium-high phosphorus iron ore. *ISIJ Int.* **2021**, *61*, 1459–1468. [\[CrossRef\]](#)
10. Kubo, H.; Matsubae-Yokoyama, K.; Nagasaka, T. Magnetic separation of phosphorus enriched phase from multiphase dephosphorization slag. *ISIJ Int.* **2010**, *50*, 59–64. [\[CrossRef\]](#)
11. Zhang, X.; Han, Y.; Sun, Y.; Li, Y. Innovative utilization of refractory iron ore via suspension magnetization roasting: A pilot-scale study. *Powder Technol.* **2019**, *352*, 16–24. [\[CrossRef\]](#)
12. Lughofer, E.; Pollak, R.; Feilmayr, C.; Schatzl, M.; Saminger-Platz, S. Prediction and explanation models for hot metal temperature, silicon concentration, and cooling capacity in ironmaking blast furnaces. *Steel Res. Int.* **2021**, *92*, 2100078. [\[CrossRef\]](#)
13. Jeong, Y.; Matsubae-Yokoyama, K.; Kubo, H.; Pak, J.; Nagasaka, T. Substance flow analysis of phosphorus and manganese correlated with South Korean steel industry. *Resour. Conserv. Recycl.* **2009**, *53*, 479–489. [\[CrossRef\]](#)
14. Dippenaar, R. Industrial uses of slag (the use and re-use of iron and steelmaking slags). *Ironmak. Steelmak.* **2005**, *32*, 35–46. [\[CrossRef\]](#)
15. Wang, L.; Guo, P.; Kong, L.; Zhao, P. Industrial application prospects and key issues of the pure-hydrogen reduction process. *Int. J. Miner. Metall. Mater.* **2022**, *29*, 1922–1931. [\[CrossRef\]](#)
16. Liu, Z.; Kobayashi, Y.; Yin, F.; Kuwabara, M.; Nagai, K. Nucleation of acicular ferrite on sulfide inclusion during rapid solidification of low carbon steel. *ISIJ Int.* **2007**, *47*, 1781–1788. [\[CrossRef\]](#)
17. Gibbs, P.J.; De Moor, E.; Merwin, M.J.; Clausen, B.; Speer, J.G.; Matlock, D.K. Austenite stability effects on tensile behavior of manganese-enriched-austenite transformation-induced plasticity steel. *Metall. Mater. Trans. A* **2011**, *42*, 3691–3702. [\[CrossRef\]](#)

18. Zurutuza, I.; Isasti, N.; Detemple, E.; Schwinn, V.; Mohrbacher, H.; Uranga, P. Effect of Nb and Mo additions in the microstructure/tensile property relationship in high strength quenched and quenched and tempered boron steels. *Metals* **2020**, *11*, 29. [\[CrossRef\]](#)
19. Yao, X.; Huang, J.; Qiao, Y.; Sun, M.; Wang, B.; Xu, B. Precipitation behavior of carbides and its effect on the microstructure and mechanical properties of 15CrNi₃MoV Steel. *Metals* **2022**, *12*, 1758. [\[CrossRef\]](#)
20. Tian, Z.; Li, B.; Zhang, X.; Jiang, Z. Double slag operation dephosphorization in BOF for producing low phosphorus steel. *J. Iron Steel Res. Int.* **2009**, *16*, 6–14. [\[CrossRef\]](#)
21. Lv, M.; Zhu, R.; Yang, L. High efficiency dephosphorization by mixed injection during steelmaking process. *Steel Res. Int.* **2019**, *90*, 1800454. [\[CrossRef\]](#)
22. Lin, L.; Zeng, J. Consideration of green intelligent steel processes and narrow window stability control technology on steel quality. *Int. J. Miner. Metall. Mater.* **2021**, *28*, 1264–1273. [\[CrossRef\]](#)
23. Qian, Q.; Dong, Q.; Xu, J.; Zhao, W.; Li, M. A metallurgical dynamics-based method for production state characterization and end-point time prediction of basic oxygen furnace steelmaking. *Metals* **2022**, *13*, 2. [\[CrossRef\]](#)
24. Li, H.; Li, X.; Liu, X.; Bu, X.; Li, H.; Lyu, Q. Industrial internet platforms: Applications in BF ironmaking. *Ironmak. Steelmak.* **2022**, *49*, 905–916. [\[CrossRef\]](#)
25. Huss, J.; Berg, M.; Kojola, N. Experimental study on phosphorus partitions between liquid iron and liquid slags based on DRI. *Metall. Mater. Trans. B* **2020**, *51*, 786–794. [\[CrossRef\]](#)
26. Wang, Z.; Bao, Y.; Wang, D.; Gu, C.; Wang, M. Study on the effect of different factors on the change of the phosphorus-rich phase in high phosphorus steel slag. *Crystals* **2022**, *12*, 1030. [\[CrossRef\]](#)
27. Ide, K.; Fruehan, R.J. Evaluation of phosphorus reaction equilibrium in steelmaking. *Iron Steelmak.* **2000**, *27*, 65–70.
28. Balajiva, K.; Quarrell, A.G.; Vajragupta, P. A laboratory investigation of the phosphorus reaction in the basic steeling process. *J. Iron Steel Inst.* **1946**, *153*, 115–150.
29. Suito, H.; Inoue, R. Thermodynamic assessment of hot metal and steel dephosphorization with MnO-containing BOF slags. *ISIJ Int.* **1995**, *35*, 258–265. [\[CrossRef\]](#)
30. Turkdogan, E.T. Assessment of P₂O₅ activity coefficients in molten slags. *ISIJ Int.* **2000**, *40*, 964–970. [\[CrossRef\]](#)
31. Sen, N. Studies on dephosphorisation of steel in induction furnace. *Steel Res. Int.* **2006**, *77*, 242–249. [\[CrossRef\]](#)
32. Assis, A.N.; Tayeb, M.A.; Sridhar, S.; Fruehan, R.J. Phosphorus equilibrium between liquid iron and CaO-SiO₂-MgO-Al₂O₃-FeO-P₂O₅ slags: EAF slags, the effect of alumina and new correlation. *Metals* **2019**, *9*, 116. [\[CrossRef\]](#)
33. Kunisada, K.; Iwai, H. Effect of Na₂O on phosphorus distribution between liquid iron and CaO-based slags. *ISIJ Int.* **2007**, *27*, 263–269. [\[CrossRef\]](#)
34. Basu, S.; Lahiri, A.K.; Seetharaman, S. A model for activity coefficient of P₂O₅ in BOF slag and phosphorus distribution between liquid steel and slag. *ISIJ Int.* **2007**, *47*, 1236–1238. [\[CrossRef\]](#)
35. Bergman, Å. Representation of phosphorus and vanadium equilibria between liquid iron and complex steelmaking type slags. *ISIJ Int.* **1988**, *28*, 945–951. [\[CrossRef\]](#)
36. Ray, H.S.; Pal, S. Simple method for theoretical estimation of viscosity of oxide melts using optical basicity. *Ironmak. Steelmak.* **2004**, *31*, 125–130. [\[CrossRef\]](#)

Disclaimer/Publisher's Note: The statements, opinions and data contained in all publications are solely those of the individual author(s) and contributor(s) and not of MDPI and/or the editor(s). MDPI and/or the editor(s) disclaim responsibility for any injury to people or property resulting from any ideas, methods, instructions or products referred to in the content.